Low-power microstructured atomic oven for alkaline-earth-like elements

J. Pick,[1,*] J. Voß,[2] S. Hirt,[2] J. Kruse,[1] T. Leopold,[1,2] R. Schwarz,[1] and C. Klempt[1]

[1] *Deutsches Zentrum für Luft- und Raumfahrt e.V., Institut für Satellitengeodäsie und Inertialsensorik, Callinstraße 30b, 30167 Hannover, Germany*

[2] *LPKF Laser & Electronics SE, Osteriede 7, 30827 Garbsen, Germany*

(Received 22 August 2024; accepted 14 November 2024; published 8 January 2025)

Alkaline-earth-like elements play pivotal roles in advanced quantum sensing technologies, notably optical clocks, with unprecedented precision achieved in recent years. Despite remarkable progress, current optical-lattice clocks still face challenges in meeting the demanding size, weight, and power consumption constraints essential for space applications. Conventional atom sources, such as ovens or dispensers, require substantial heating power, which makes up a significant fraction of the overall power consumption of the system. Addressing this challenge, we present a microstructured atomic oven based on fused silica, designed for miniaturization and low-power operation. We characterize the oven by loading a magneto-optical trap with Yb evaporated from the oven and demonstrate operation with a loading rate above 10^8 atoms/s for heating powers below 250 mW.

DOI: 10.1103/PhysRevApplied.23.014020

I. INTRODUCTION

Alkaline-earth-like elements are employed in state-of-the-art quantum sensors, most prominently optical clocks [1,2], and in quantum computing with neutral atoms [3,4] or trapped ions [5]. Rapid technological advancement has enabled the operation of optical clocks with fractional frequency uncertainties in the low-10^{-18} range [6–11] and the development of transportable systems aiming to field deployment [12–15] or even reaching out into space [16,17], where numerous applications for optical lattice clocks have been proposed [18,19].

The maturity of present-day optical lattice clocks is still insufficient to meet the stringent requirements of a space flight in terms of size, weight, and power consumption (SWaP). Field-deployable systems, either on the ground or in space, therefore require significant miniaturization of key components. For alkaline-earth-like elements, conventional atom sources are based on an oven [20–22] or dispensers [23–26] that require heating to temperatures up to 400–500°C in order to provide a sufficient flux of atoms, where typical heating powers of several tens of watts are required. The evaporated atoms are then generally trapped and cooled in a magneto-optical trap (MOT) as a first step in the preparation of ultracold atoms. In transportable experiments, the required heating power of the source can be a significant portion of the overall power consumption of the system [17].

A mitigating technique in the reduction of thermal losses due to convection is by using in-vacuum heating [20], leaving thermal radiation and conduction as the remaining loss processes. However, the required heating power still remains in the order of tens of watts. Progress toward the reduction of thermal conduction has been made with a chip-size atomic oven based on silicon, which is suspended by narrow beams [27]. The achievable reduction of thermal conduction has, however, been limited due to the decreasing mechanical robustness with reduced beam thickness.

In this paper, we present a miniaturized monolithic in-vacuum atomic oven based on microstructured fused silica. Compared to silicon, fused silica offers a reduction of thermal conductance by 2 orders of magnitude. The oven has been manufactured by laser-induced deep etching (LIDE). The monolithic design holds a spring-mounted reservoir that contains the atoms and is heated directly. A laser-structured electrical circuit allows for electrical heating as well as heating by optical absorption of light. While evaporation of alkaline-earth-like atoms by optical illumination has already been demonstrated [28,29], our design relaxes the optical-power requirement and enables continuous operation without the need for a regular realignment of the optical heating beam. The geometry of the mounting springs offers optimal thermal insulation of the reservoir from the mounting structure as well as mechanical stability

*Contact author: julian.pick@dlr.de

with respect to differential thermal expansion along the springs themselves. Thus, thermal radiation remains as the only significant loss process at high temperatures, enabling oven operation at low power consumption. Compared to conventional atomic beam ovens, our approach drastically reduces the size and weight. Therefore, it can be placed directly near the structure that generates the MOT. Although our atomic reservoir is likewise smaller compared to classical oven designs, we expect a sufficient lifetime on the order of multiple years, since the atomic flux into the MOT volume is comparable at much lower oven temperatures, i.e., atomic evaporation rates. For both heating options, we demonstrate a power consumption far below 1 W for generating a fast-loading MOT with more than 10^8 atoms/s.

We compare the two heating mechanisms that the oven features and characterize its atom-evaporation properties by measuring the MOT loading dynamics. Our oven is specifically well suited to operate modern compact single-beam MOT structures [30–35], which further miniaturize a crucial component of modern quantum sensors, paving the way toward space-borne applications.

II. OVEN DESIGN

The atomic oven is depicted in Fig. 1. It is based on a circular fused silica chip that is manufactured in larger numbers from a 6-in. fused silica wafer with a 500-μm initial thickness. An outer support structure of 13 mm diameter holds the central part via four double-folded mounting springs, each with a cross section of 150 μm × 450 μm and a length of 6 mm. The central part of the oven is a heating plate with a 4-mm outer diameter and a 3-mm-wide recess. It can be filled with alkaline-earth-like atoms and it is the only part of the chip that is heated in order to evaporate the atoms.

The suspension of the heating plate in the chip using springs is a key feature in the thermal isolation of the heating plate toward the mounting structure. It minimizes heat conductance from the heating plate to the outside part of the chip, due to its favorable aspect ratio between cross section and length. Furthermore, it ensures mechanical stability with respect to thermal expansion along the spring, which would introduce mechanical stress and out-of-plane bending in a straight connection due to the expected large temperature gradient between the mounting structure and the heating plate. The chips have been fabricated using the two-step LIDE technology developed by LPKF [36]. In the first step, the glass is laser modified and in the second, it is chemically etched with a hydrofluoric-acid-based solution. The laser-modified areas etch at a significantly higher rate than the unmodified ones, enabling the formation of high-aspect-ratio structures with a precisely defined geometry without introducing defects into the glass. The defect-free manufacturing process provides the mechanical stability needed for this application. During the etching process, the overall substrate thickness is reduced to about 450 μm, which has been taken into account in the design of the heating plate.

The back side of the chip has been metallized in a physical-vapor-deposition (PVD) process to enable electrical heating with a 300-nm platinum layer on a 10-nm titanium adhesion layer. A heating structure, in the shape of a Fermat's spiral, has been manufactured by removing a 15-μm-wide strip of the metal layer via laser scribing, creating electrical insulation between neighboring windings. The remaining conductive path along the spiral is approximately 65 μm wide, with a total length of about 84 mm. Each end of the spiral is split into two parallel paths, where the conductor length difference for two parallel connections is about 2.5 mm. Each path is terminated by a copper contact pad. Two of the copper pads (1 and 4 in Fig. 1) are connected to an electric power source for electrical heating, while the other two (contact pads 2 and 3) are used for measuring the voltage drop along the spiral, enabling a four-point resistance measurement, to determine the temperature of the spiral. Apart from the electrical heating, the reservoir can also be heated by optical illumination. For that, the Pt filling between the lanes, which has not been removed, maximizes the area that effectively absorbs the heating light. The bottom of the reservoir separates the heated Pt layer from the atoms. In order to ensure sufficient heat transfer without compromising mechanical stability, it has a thickness of 30 μm.

When the oven is operated in vacuum, the power consumption is determined by losses due to thermal radiation and thermal conduction, where the thermal radiation is described by the Stefan-Boltzmann law and the thermal conduction by Fourier's law. For our oven geometry, we calculate an estimate of the total power consumption as a function of the heating-plate temperature, which is shown in Fig. 2. It can be seen that for temperatures above 100°C, the total power loss is dominated by thermal radiation, since heat conduction through the mounting springs is suppressed due to their geometry and the material properties of fused silica.

Due to the comparably small volume of the reservoir, of only about 3 mm^3, a critical design parameter is the oven lifetime, which refers to the duration for which it can sustain a decent flux of atoms before the reservoir becomes empty. At a given oven temperature, the lifetime can be directly calculated from the expected evaporation rate of the specific element that is used. We have calculated the vapor pressure p_v using [37]

$$\log(p_v) = A/T + B\log(T) + CT + D, \tag{1}$$

with parameters A, B, C, and D taken from the literature for Yb and Sr. The corresponding evaporation rate at

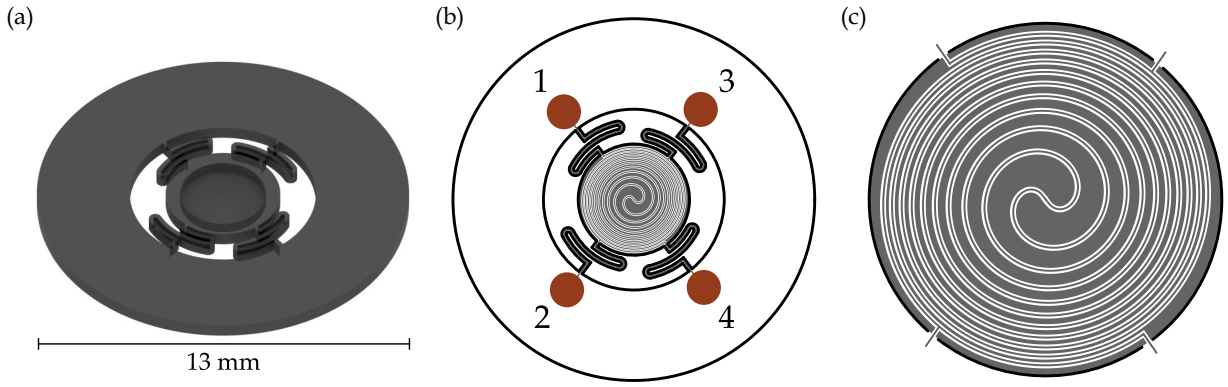

FIG. 1. The design of the monolithic microstructured fused-silica oven. (a) A rendered image of the front side, showing the spring-mounted reservoir in the center. (b) A sketch of the back side. The numbered brown circles indicate copper contact pads and the gray lines represent the platinum layer. (c) An enlarged view of the back side of the heating plate. Here, the high platinum filling factor supports light absorption for improved optical heating from the back side. Not shown are the mounting springs and the outside part of the chip.

temperature T is given by the Hertz-Knudsen equation,

$$\dot{n}(T) = \frac{p_v(T)}{\sqrt{2\pi MRT}} N_a, \tag{2}$$

where M is the molecular mass, R the ideal gas constant, and N_a is Avogadro's constant. From the specific evaporation rates, we can also estimate the MOT loading rate that can be achieved. Here, the small oven size emerges as a key advantage, enabling us to place it directly next to the MOT volume and thus gaining a comparably large geometric acceptance angle for evaporated atoms to enter the MOT trapping volume. In the setup described in Sec. III, the half-opening angle for which atoms can enter the MOT volume is about 22°. Furthermore, we assume a maximum MOT capture velocity of our pyramid MOT of 40 m/s. From this, we estimate the MOT loading rates of the most abundant isotopes of the alkaline-earth-like elements ^{174}Yb and ^{88}Sr for different temperatures of the evaporated atoms. They are shown in Fig. 3, together with the expected lifetimes of a reservoir with an initial filling of 30 mg. It is evident that for both elements, continuous operation with MOT loading rates above 10^8 atoms/s for a number of years is possible. Furthermore, the lifetime increases drastically when the oven is operated at a lower temperature, yielding more conservative loading rates, or when the oven is not operated continuously. An even higher lifetime could be reached by redesigning the oven with a larger reservoir, at the cost of slower heating dynamics and an increase of the overall size and weight.

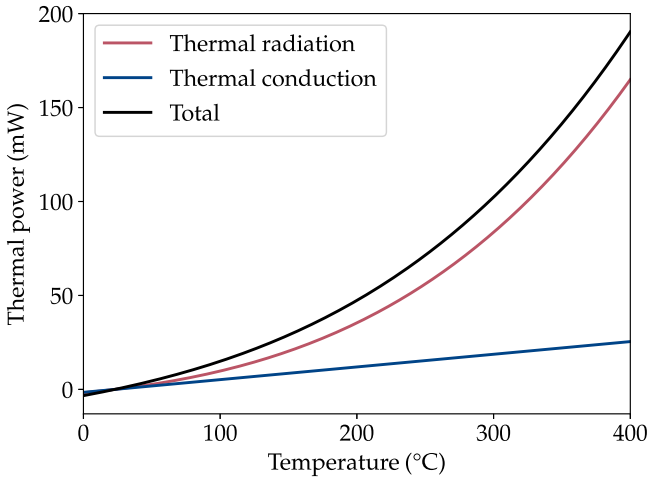

FIG. 2. The estimated thermal power loss as a function of the temperature of the heating plate.

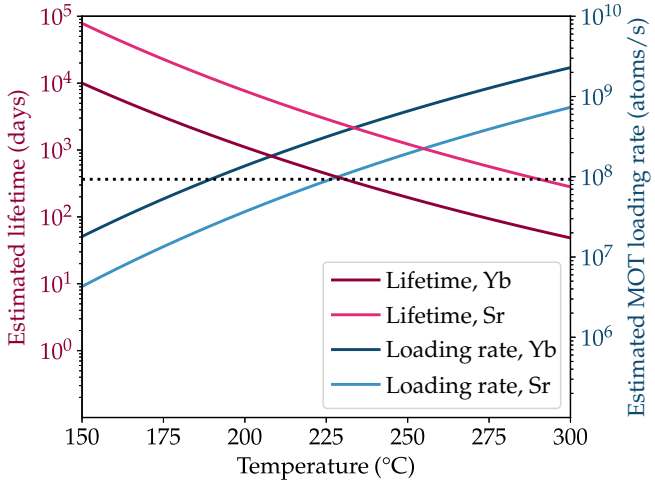

FIG. 3. The estimated oven lifetime and MOT loading rate as a function of the temperature for Yb and Sr. The black dotted line indicates a lifetime of 1 year. The MOT loading rates are given for the most abundant isotopes, ^{174}Yb and ^{88}Sr.

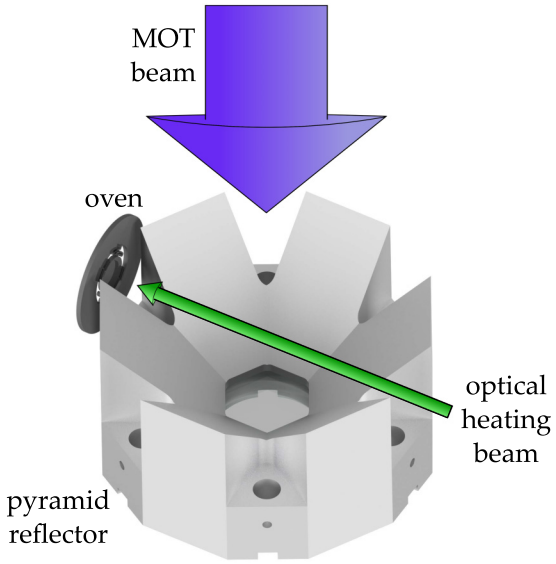

FIG. 4. The experimental setup for the characterization of the oven.

The reservoir can be filled by evaporation of atoms from an external source and subsequent deposition on the glass substrate [27,38], but for the results described in the following we have instead placed a solid block of ytterbium with a weight of approximately 30 mg onto the reservoir. A thin layer of indium foil has been added between the Yb block and the reservoir, in order to improve the thermal contact with the heating plate and thus reduce the required electrical heating power.

III. RESULTS

We have tested the oven by loading a MOT generated by a pyramid reflector [39], which only requires a single incident laser beam. The reflector is a quasimonolithic aluminum structure and is described in detail in Ref. [40]. It features six angled reflective surfaces to generate beams for radial trapping and a bichromatic wave plate with a highly reflective coating on its back side for axial trapping. Gaps between the reflective surfaces allow for radial optical access and atom loading. The oven is placed directly at such a gap, at a distance of approximately 1 mm from the outside of the reflector, as indicated in Fig. 4. This enables atoms that are evaporated from the oven under a large solid angle to enter the trap volume. The exact position of the oven and distance to the pyramid can be adjusted with a port aligner.

For electrical heating, we have applied a voltage between connections 1 and 4 and simultaneously measured the voltage drop across connections 2 and 3. We have measured a room-temperature resistance of the spiral of 523 Ω. However, it has been observed that the resistance does not increase monotonously with increasing heating power and so it is not possible to determine the temperature from the measured resistance.

The gap in the pyramid opposite the oven is used for coupling in a beam at 556 nm for optical heating. The optical heating beam has a diameter of 4 mm, so that the reservoir is fully illuminated. With this optical heating setup, the Yb is heated directly by absorbing the 556-nm light, instead of the Pt layer, which has a low absorptance at this wavelength. We have chosen this setup because direct illumination of the Yb block has been easier due to the good optical access through the pyramid. In this case, the oven is not used directly for heating but still ensures thermal isolation from the environment for a low power requirement on the heating beam. Direct heating of the Pt layer would require a lower wavelength for efficient optical absorption. The optical heating beam is far detuned from the atomic transition at 556 nm to avoid slowing of the atoms due to this beam, which could potentially enhance the MOT loading rate.

The magnetic quadrupole field that is required for MOT operation is generated by two coils in anti-Helmholtz configuration, which are wound on two water-cooled copper mounts. The magnetic field gradient was 3.3 mT/cm in the axial direction for all measurements. A single laser beam at 399 nm is incident on the pyramid reflector and is split and reflected into all required beams for three-dimensional trapping and cooling. We have chosen a collimated Gaussian beam with a $1/e^2$ diameter of 45 mm, which is larger than the 34-mm outer diameter of the pyramid.

We have loaded a MOT operating on the broad $^1S_0 \rightarrow {}^1P_1$ transition at 399 nm. We have measured the MOT loading curves of the most abundant isotope ^{174}Yb for different electrical and optical heating powers. The optical power for the MOT at 399 nm was 60 mW and the MOT detuning was −32 MHz. Exemplary loading curves are shown in Fig. 5. Here, the error bars indicate statistical fluctuations and represent one standard deviation. The solid lines are exponential fits that yield the respective loading rates and settling times. Here, the settling time is equivalent to the inverse of the atomic loss rate in the fully loaded MOT. Both parameters are shown for different heating powers in Fig. 6. It is evident that with both heating mechanisms, loading rates above 10^8 atoms/s can be achieved with heating powers below 250 mW. This comparably large MOT loading rate at a moderate estimated oven temperature highlights the advantage of the oven, in that it can be placed close to the trapping volume due to its small size. In order to achieve the same loading rates, the required power for electrical heating is larger than for optical heating. This is due to the limited thermal contact between the Yb block and the reservoir, which is advantageous when the Yb is directly heated by the optical beam and disadvantageous for electrical heating of the reservoir. Nevertheless, electrical heating is potentially the more power-efficient approach, since the generation of

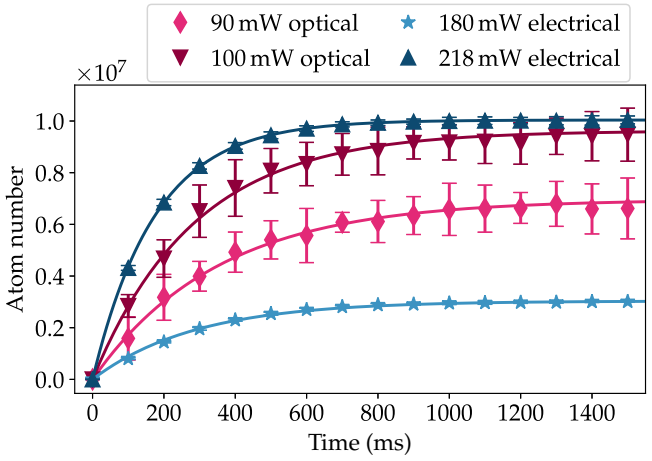

FIG. 5. Exemplary MOT loading curves for different optical and electrical heating powers.

laser light requires more electrical power than the optical output power that is available for heating. For both heating mechanisms, the MOT lifetime decreases with increasing heating power. This can be explained by collisions of the trapped atoms with fast atoms emerging from the oven, which limit the lifetime and scale with the heating power.

We have investigated the heating dynamics of the oven by repeatedly loading a MOT and measuring the loading rate. Starting at room temperature, we have turned on the electrical or optical heating with powers of 205 mW and 100 mW, respectively, and tracked the loading rate for a duration of 20 min. The result is shown in Fig. 7. For the electrical heating, the loading rate increases strongly within the first 2 min and then increases further slowly over the course of the whole measurement. For the optical heating, the loading rate also increases strongly during the first 2 min but then it oscillates. This periodic oscillation can

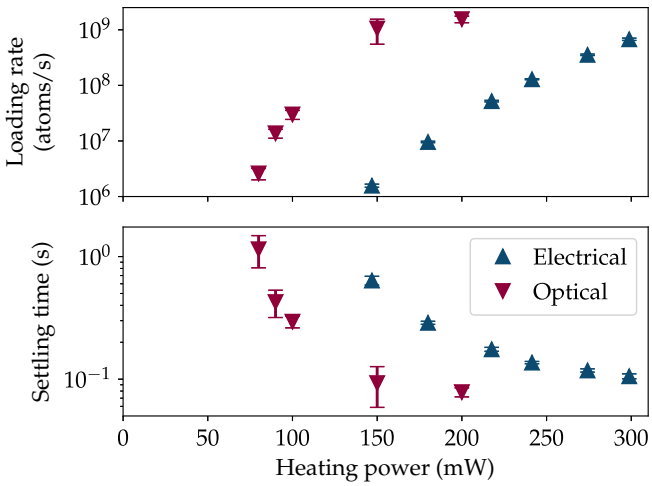

FIG. 6. MOT loading rates and settling times as a function of the heating power for both heating mechanisms.

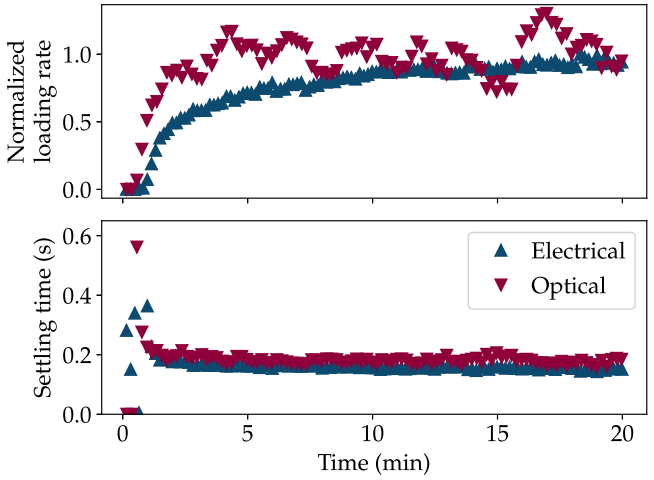

FIG. 7. The heating dynamics of the oven with electrical and optical heating. The MOT loading rates for electrical heating are normalized to the maximal value and for the optical heating they are normalized to the mean value in the interval between 5 min and 20 min.

be associated with power fluctuations of the optical heating beam, which is why it does not appear for the electrical heating. This means that the electrical heating generates a far more stable flux of atoms compared to the optical heating, when the optical heating power is not actively stabilized.

The velocities of the atoms that are evaporated from the oven are described by a thermal distribution. Due to the high temperature that is required for evaporation, it can be assumed that only a small fraction of the atoms is slow enough to be captured by the MOT. It can thus be expected that the MOT capture velocity, which can be enhanced by increasing the MOT power, has a strong influence on the loading rate. For a fixed electrical heating power of 205 mW, we have measured the loading rate as a function of the MOT power. Additionally to ^{174}Yb, the fermionic isotope ^{171}Yb is of interest, since it is commonly used in optical lattice clocks. We have performed the measurement for both isotopes (Fig. 8). It can be seen that the respective loading rates increase strongly with increasing MOT power. The loading rates for the fermionic isotope are lower due to its lower natural abundance. Nevertheless, it can be seen that a high loading rate of ^{171}Yb can be achieved with the MOT powers that are typically available from commercial laser sources.

When the oven is heated with an electrical power of 205 mW, the pressure inside the vacuum chamber rises to 5×10^{-10} mBar. Although the fast atoms evaporating from the oven can collide with the trapped atoms, it is possible to efficiently transfer the atoms to the second MOT stage operating on the narrow $^1S_0 \rightarrow {}^3P_1$ transition at 556 nm. The MOT beam at 556 nm is incident on the pyramid reflector through the same optical path as the first-stage

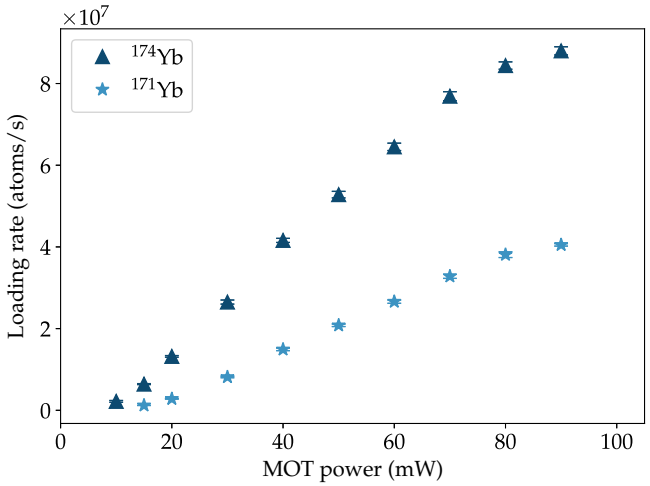

FIG. 8. The MOT loading rate as a function of the MOT power at 399 nm for both relevant isotopes, ^{174}Yb and ^{171}Yb. The electrical heating power was 205 mW and the MOT detuning was −32 MHz.

MOT beam, resulting in the same beam diameter. In order to characterize the second MOT stage, we first load a MOT on the first-stage transition. We then switch on the 556-nm light and after a transfer time of 20 ms, we turn off the 399-nm light. After a variable holding time, we transfer the atoms back into the first MOT stage and compare the initial and final atom numbers. This atom-number ratio is measured for different holding times in the second MOT stage, so that the initial transfer efficiency and the lifetime can be determined. We have repeated this measurement for different detunings of the 556-nm laser (Fig. 9), which had an optical power of 10 mW. It is evident that a transfer efficiency above 90% is possible, which shows that the oven

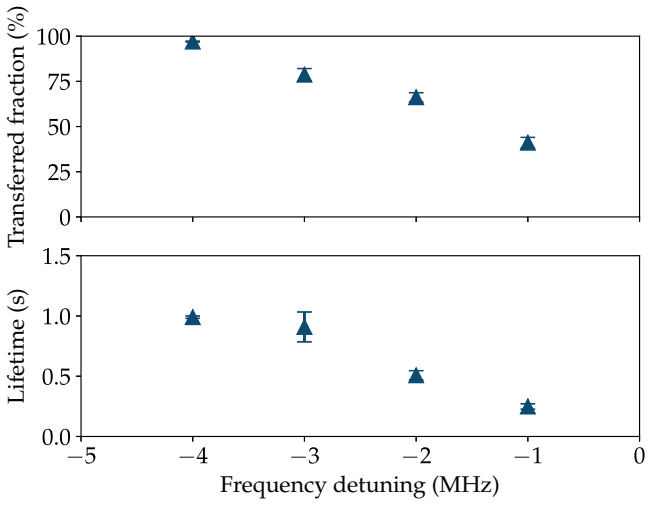

FIG. 9. The transfer efficiency and lifetime in the second MOT stage as a function of the frequency detuning of the 556-nm MOT laser.

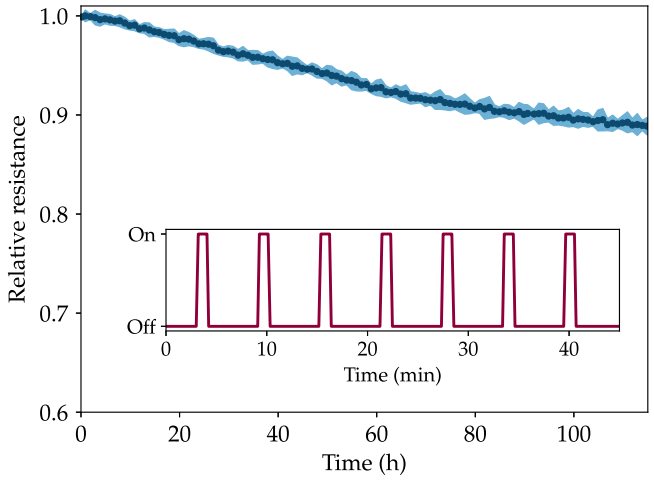

FIG. 10. The relative resistance of the heating spiral during a repeated heating and cooling cycle. The dark blue points represent hourly averaged resistances and the light blue shaded area describes the corresponding standard deviation. The inset shows the heating sequence for a fraction of the total measurement time: "On" and "Off" refer to whether or not the electrical heating is active.

is ideally suited to serve as an atom source for a compact optical lattice clock.

To investigate the long-term characteristics of the oven, we have operated it continuously over the course of 11 days with MOT loading rates exclusively above 10^7 atoms/s. We have observed no visible reduction of the size of the Yb block, suggesting a reasonably long lifetime of the oven at the given loading rate. However, we have observed an increase in the required optical heating power to maintain our target loading rate. We attribute this to an observed coating of the wave plate inside the pyramid due to the evaporated ytterbium from the oven. Such a coating of the optical surfaces might be avoided by blocking the direct line of sight from the oven with a shutter, by generating a collimated atomic beam emerging from the oven with a nozzle [41], or by implementing a 2D-MOT. Furthermore, we have investigated the robustness of the oven during repeated temperature changes. We have performed more than 1100 repetitions of heating the oven with 200-mW electrical power for 1 min followed by 5 min of cool-down time. We have measured the oven resistance during the heating (Fig. 10). While we have observed a slow reduction of the observed resistance, stable long-term operation can be achieved by stabilizing the electrical power instead of the current. We attribute the reduction of the resistance to either a slow heating of the peripheral infrastructure or an annealing effect of the thin Pt layer.

IV. CONCLUSIONS

We have presented a low-SWaP oven for alkaline-earth-like elements and characterized it by loading a MOT

generated with a pyramid reflector. The defect-free microstructuring of fused silica using the LIDE process has been a key technology to achieve the presented results. Starting from room temperature, the oven takes less than 5 min to heat up to a temperature that yields a large MOT loading rate. For MOT loading rates above 10^8 atoms/s, it requires less than 250 mW electrical heating power or less than 150 mW optical heating power. While electrical heating leads to a stable flux of atoms, the MOT loading rate measured with optical heating fluctuates due to power fluctuations of the heating beam. We have demonstrated that a MOT of the most abundant isotope, ^{174}Yb, as well as the clock-relevant isotope ^{171}Yb, can be loaded and that transfer to the second MOT stage is possible, with a transfer efficiency above 90%. The oven thus constitutes a promising candidate to serve as an atom source for a future transportable optical lattice clock. Possible modifications of the oven design would allow us to adjust key parameters. The heating time can be reduced by modifying the mounting springs for an increased heat conductance, at the cost of a higher power consumption. A trade-off between the oven lifetime and the heating time can be chosen by varying the size of the reservoir.

ACKNOWLEDGMENTS

We thank J. Koch for fruitful discussions about the oven design and operation. We acknowledge funding from the joint project "Innovative Vacuum Technology for Quantum Sensors" (InnoVaQ), funded by the German Federal Ministry of Education and Research (BMBF) as part of the funding program "Quantum Technologies—from Basic Research to Market" (Contracts No. 13N15915 and No. 13N15916). We further acknowledge funding by the Deutsche Forschungsgemeinschaft (DFG, German Research Foundation) under Germany's Excellence Strategy—EXC-2123 QuantumFrontiers—390837967.

[1] M. Takamoto, F.-L. Hong, R. Higashi, and H. Katori, An optical lattice clock, Nature **435**, 321 (2005).

[2] A. D. Ludlow, M. M. Boyd, J. Ye, E. Peik, and P. O. Schmidt, Optical atomic clocks, Rev. Mod. Phys. **87**, 637 (2015).

[3] A. Jenkins, J. W. Lis, A. Senoo, W. F. McGrew, and A. M. Kaufman, Ytterbium nuclear-spin qubits in an optical tweezer array, Phys. Rev. X **12**, 021027 (2022).

[4] S. Ma, A. P. Burgers, G. Liu, J. Wilson, B. Zhang, and J. D. Thompson, Universal gate operations on nuclear spin qubits in an optical tweezer array of ^{171}Yb atoms, Phys. Rev. X **12**, 021028 (2022).

[5] C. D. Bruzewicz, J. Chiaverini, R. McConnell, and J. M. Sage, Trapped-ion quantum computing: Progress and challenges, Appl. Phys. Rev. **6**, 021314 (2019).

[6] I. Ushijima, M. Takamoto, M. Das, T. Ohkubo, and H. Katori, Cryogenic optical lattice clocks, Nat. Photonics **9**, 185 (2015).

[7] W. F. McGrew, X. Zhang, R. J. Fasano, S. A. Schäffer, K. Beloy, D. Nicolodi, R. C. Brown, N. Hinkley, G. Milani, M. Schioppo, T. H. Yoon, and A. D. Ludlow, Atomic clock performance enabling geodesy below the centimetre level, Nature **564**, 87 (2018).

[8] T. Bothwell, D. Kedar, E. Oelker, J. M. Robinson, S. L. Bromley, W. L. Tew, J. Ye, and C. J. Kennedy, JILA SrI optical lattice clock with uncertainty of 2.0×10^{-18}, Metrologia **56**, 065004 (2019).

[9] S. M. Brewer, J.-S. Chen, A. M. Hankin, E. R. Clements, C. W. Chou, D. J. Wineland, D. B. Hume, and D. R. Leibrandt, $^{27}Al^+$ quantum-logic clock with a systematic uncertainty below 10^{-18}, Phys. Rev. Lett. **123**, 033201 (2019).

[10] Y. Huang, B. Zhang, M. Zeng, Y. Hao, Z. Ma, H. Zhang, H. Guan, Z. Chen, M. Wang, and K. Gao, Liquid-nitrogen-cooled Ca^+ optical clock with systematic uncertainty of 3×10^{-18}, Phys. Rev. Appl. **17**, 034041 (2022).

[11] A. Tofful, C. F. A. Baynham, E. A. Curtis, A. O. Parsons, B. I. Robertson, M. Schioppo, J. Tunesi, H. S. Margolis, R. J. Hendricks, J. Whale, R. C. Thompson, and R. M. Godun, $^{171}Yb^+$ optical clock with 2.2×10^{-18} systematic uncertainty and absolute frequency measurements, Metrologia **61**, 045001 (2024).

[12] S. B. Koller, J. Grotti, S. Vogt, A. Al-Masoudi, S. Dörscher, S. Häfner, U. Sterr, and C. Lisdat, Transportable optical lattice clock with 7×10^{-17} uncertainty, Phys. Rev. Lett. **118**, 073601 (2017).

[13] R. J. Fasano, Ph.D. thesis, Graduate School of the University of Colorado, University of Colorado, 2021.

[14] N. Ohmae, M. Takamoto, Y. Takahashi, M. Kokubun, K. Araki, A. Hinton, I. Ushijima, T. Muramatsu, T. Furumiya, Y. Sakai, N. Moriya, N. Kamiya, K. Fujii, R. Muramatsu, T. Shiimado, and H. Katori, Transportable strontium optical lattice clocks operated outside laboratory at the level of 10^{-18} uncertainty, Adv. Quantum Technol. **4**, 2100015 (2021).

[15] Y. Huang, H. Zhang, B. Zhang, Y. Hao, H. Guan, M. Zeng, Q. Chen, Y. Lin, Y. Wang, S. Cao, K. Liang, F. Fang, Z. Fang, T. Li, and K. Gao, Geopotential measurement with a robust, transportable Ca^+ optical clock, Phys. Rev. A **102**, 050802 (2020).

[16] S. Origlia, M. S. Pramod, S. Schiller, Y. Singh, K. Bongs, R. Schwarz, A. Al-Masoudi, S. Dörscher, S. Herbers, S. Häfner, U. Sterr, and C. Lisdat, Towards an optical clock for space: Compact, high-performance optical lattice clock based on bosonic atoms, Phys. Rev. A **98**, 053443 (2018).

[17] Y. Chen, C. Zhou, W. Tan, F. Guo, G. Zhao, J. Xia, J. Meng, and H. Chang, Development of compact and robust physical system for strontium optical lattice clock, Appl. Sci. **14**, 1551 (2024).

[18] A. Derevianko, K. Gibble, L. Hollberg, N. R. Newbury, C. Oates, M. S. Safronova, L. C. Sinclair, and N. Yu, Fundamental physics with a state-of-the-art optical clock in space, Quantum Sci. Technol. **7**, 044002 (2022).

[19] V. Schkolnik, D. Budker, O. Fartmann, V. Flambaum, L. Hollberg, T. Kalaydzhyan, S. Kolkowitz, M. Krutzik, A. Ludlow, N. Newbury, C. Pyrlik, L. Sinclair, Y. Stadnik, I.

Tietje, J. Ye, and J. Williams, Optical atomic clock aboard an Earth-orbiting space station (OACESS): Enhancing searches for physics beyond the standard model in space, Quantum Sci. Technol. **8**, 014003 (2023).

[20] M. Schioppo, N. Poli, M. Prevedelli, S. Falke, C. Lisdat, U. Sterr, and G. M. Tino, A compact and efficient strontium oven for laser-cooling experiments, Rev. Sci. Instrum. **83**, 103101 (2012).

[21] B. Song, Y. Zou, S. Zhang, C.-w. Cho, and G.-B. Jo, A cost-effective high-flux source of cold ytterbium atoms, Appl. Phys. B **122**, 250 (2016).

[22] E. Wodey, R. J. Rengelink, C. Meiners, E. M. Rasel, and D. Schlippert, A robust, high-flux source of laser-cooled ytterbium atoms, J. Phys. B: At., Mol. Opt. Phys. **54**, 035301 (2021).

[23] E. M. Bridge, J. Millen, C. S. Adams, and M. P. A. Jones, A vapor cell based on dispensers for laser spectroscopy, Rev. Sci. Instrum. **80**, 013101 (2009).

[24] S. Dörscher, A. Thobe, B. Hundt, A. Kochanke, R. Le Targat, P. Windpassinger, C. Becker, and K. Sengstock, Creation of quantum-degenerate gases of ytterbium in a compact 2D-/3D-magneto-optical trap setup, Rev. Sci. Instrum. **84**, 043109 (2013).

[25] M. Kwon, A. Holman, Q. Gan, C.-W. Liu, M. Molinelli, I. Stevenson, and S. Will, Jet-loaded cold atomic beam source for strontium, Rev. Sci. Instrum. **94**, 013202 (2023).

[26] J. Nomura, T. Momma, Y. Kojima, Y. Hisai, T. Kobayashi, D. Akamatsu, and F.-L. Hong, Direct loading of Yb atoms into a 3D magneto-optical trap from a dispenser atomic source, AIP Adv. **13**, 025361 (2023).

[27] P. D. D. Schwindt, Y.-Y. Jau, H. Partner, A. Casias, A. R. Wagner, M. Moorman, R. P. Manginell, J. R. Kellogg, and J. D. Prestage, A highly miniaturized vacuum package for a trapped ion atomic clock, Rev. Sci. Instrum. **87**, 053112 (2016).

[28] O. Kock, W. He, D. Świerad, L. Smith, J. Hughes, K. Bongs, and Y. Singh, Laser controlled atom source for optical clocks, Sci. Rep. **6**, 37321 (2016).

[29] M. Yasuda, T. Tanabe, T. Kobayashi, D. Akamatsu, T. Sato, and A. Hatakeyama, Laser-controlled cold ytterbium atom source for transportable optical clocks, J. Phys. Soc. Jpn. **86**, 125001 (2017).

[30] M. Vangeleyn, P. F. Griffin, E. Riis, and A. S. Arnold, Single-laser, one beam, tetrahedral magneto-optical trap, Opt. Express **17**, 13601 (2009).

[31] M. Vangeleyn, P. F. Griffin, E. Riis, and A. S. Arnold, Laser cooling with a single laser beam and a planar diffractor, Opt. Lett. **35**, 3453 (2010).

[32] W. Bowden, R. Hobson, I. R. Hill, A. Vianello, M. Schioppo, A. Silva, H. S. Margolis, P. E. G. Baird, and P. Gill, A pyramid MOT with integrated optical cavities as a cold atom platform for an optical lattice clock, Sci. Rep. **9**, 11704 (2019).

[33] A. Sitaram, P. K. Elgee, G. K. Campbell, N. N. Klimov, S. Eckel, and D. S. Barker, Confinement of an alkaline-earth element in a grating magneto-optical trap, Rev. Sci. Instrum. **91**, 103202 (2020).

[34] S. Bondza, C. Lisdat, S. Kroker, and T. Leopold, Two-color grating magneto-optical trap for narrow-line laser cooling, Phys. Rev. Appl. **17**, 044002 (2022).

[35] S. A. Bondza, T. Leopold, R. Schwarz, and C. Lisdat, Achromatic, planar Fresnel-reflector for a single-beam magneto-optical trap, Rev. Sci. Instrum. **95**, 013202 (2024).

[36] R. Ostholt, N. Ambrosius, and R. A. Kruger, in *Proceedings of the 5th Electronics System-integration Technology Conference (ESTC)* (IEEE, Helsinki, Finland, 2014), p. 1.

[37] J. Safarian and T. A. Engh, Vacuum evaporation of pure metals, Metall. Mater. Trans. A **44**, 747 (2013).

[38] R. P. Manginell, M. W. Moorman, J. M. Anderson, G. R. Burns, K. E. Achyuthan, D. R. Wheeler, and P. D. D. Schwindt, *In situ* dissolution or deposition of ytterbium (Yb) metal in microhotplate wells for a miniaturized atomic clock, Opt. Express **20**, 24650 (2012).

[39] K. I. Lee, J. A. Kim, H. R. Noh, and W. Jhe, Single-beam atom trap in a pyramidal and conical hollow mirror, Opt. Lett. **21**, 1177 (1996).

[40] J. Pick, R. Schwarz, J. Kruse, C. Lisdat, and C. Klempt, Compact structures for single-beam magneto-optical trapping of ytterbium, Rev. Sci. Instrum. **95**, 073201 (2024).

[41] R. Senaratne, S. V. Rajagopal, Z. A. Geiger, K. M. Fujiwara, V. Lebedev, and D. M. Weld, Effusive atomic oven nozzle design using an aligned microcapillary array, Rev. Sci. Instrum. **86**, 023105 (2015).